The C3a Anaphylatoxin Receptor Is a Key Mediator of Insulin Resistance and Functions by Modulating Adipose Tissue Macrophage Infiltration and Activation

Yaël Mamane,[1] Chi Chung Chan,[1] Genevieve Lavallee,[1] Nicolas Morin,[1] Li-Jing Xu,[1] JingQi Huang,[1] Robert Gordon,[1] Winston Thomas,[2] John Lamb,[3] Eric E. Schadt,[3] Brian P. Kennedy,[1] and Joseph A. Mancini[1]

OBJECTIVE—Significant new data suggest that metabolic disorders such as diabetes, obesity, and atherosclerosis all posses an important inflammatory component. Infiltrating macrophages contribute to both tissue-specific and systemic inflammation, which promotes insulin resistance. The complement cascade is involved in the inflammatory cascade initiated by the innate and adaptive immune response. A mouse genomic F2 cross biology was performed and identified several causal genes linked to type 2 diabetes, including the complement pathway.

RESEARCH DESIGN AND METHODS—We therefore sought to investigate the effect of a C3a receptor (C3aR) deletion on insulin resistance, obesity, and macrophage function utilizing both the normal-diet (ND) and a diet-induced obesity mouse model.

RESULTS—We demonstrate that high C3aR expression is found in white adipose tissue and increases upon high-fat diet (HFD) feeding. Both adipocytes and macrophages within the white adipose tissue express significant amounts of C3aR. C3aR$^{-/-}$ mice on HFD are transiently resistant to diet-induced obesity during an 8-week period. Metabolic profiling suggests that they are also protected from HFD-induced insulin resistance and liver steatosis. C3aR$^{-/-}$ mice had improved insulin sensitivity on both ND and HFD as seen by an insulin tolerance test and an oral glucose tolerance test. Adipose tissue analysis revealed a striking decrease in macrophage infiltration with a concomitant reduction in both tissue and plasma proinflammatory cytokine production. Furthermore, C3aR$^{-/-}$ macrophages polarized to the M1 phenotype showed a considerable decrease in proinflammatory mediators.

CONCLUSIONS—Overall, our results suggest that the C3aR in macrophages, and potentially adipocytes, plays an important role in adipose tissue homeostasis and insulin resistance. ***Diabetes*** **58:2006–2017, 2009**

From the [1]Department of Biochemistry and Molecular Biology, Merck Frosst Centre for Therapeutic Research, Kirkland, Quebec, Canada; [2]Deltagen, San Mateo, California; and [3]Rosetta Inpharmatics, Merck, Seattle, Washington.
Corresponding author: Yael Mamane, yael_mamane@merck.com, or Joseph A. Mancini, joseph_mancini@merck.com.
Received 4 March 2009 and accepted 12 June 2009.
Published ahead of print at http://diabetes.diabetesjournals.org on 6 July 2009. DOI: 10.2337/db09-0323.
G.L. and N.M. contributed equally to this article.

The complement system is an integral part of both the innate and adaptive immune response involved in the defense against invading pathogens (1). Complement activation culminates in a massive amplification of the immune response leading to increased cell lysis, phagocytosis, and inflammation (1). C3 is the most abundant component of the complement cascade and the convergent point of all three major complement activation pathways. C3 is cleaved into C3a and C3b by the classical and lectin pathways, and iC3b is generated by the alternative pathway (2,3). C3a has potent anaphylatoxin activity, directly triggering degranulation of mast cells, inflammation, chemotaxis, activation of leukocytes, as well as increasing vascular permeability and smooth muscle contraction (3). C3a mediates its downstream signaling effects by binding to the C3a receptor (C3aR), a Gi-coupled G protein–coupled receptor. Several studies have demonstrated a role for C3a and C3aR in asthma, sepsis, liver regeneration, and autoimmune encephalomyelitis (1,3). Therefore, targeting C3aR may be an attractive therapeutic option for the treatment of several inflammatory diseases.

Increasing literature suggests that metabolic disorders such as diabetes, obesity, and atherosclerosis also possess an important inflammatory component (4–7). Several seminal reports have demonstrated that resident macrophages can constitute as much as 40% of the cell population of adipose tissue (7–9) and can significantly affect insulin resistance (10–18). Several proinflammatory cytokines, growth factors, acute-phase proteins, and hormones are produced by the adipose tissue and implicated in insulin resistance and vascular homeostasis (4–7,19). An integrated genomics approach was performed with several mouse strains to infer causal relationships between gene expression and complex genetic diseases such as obesity/diabetes. This approach identified the *C3aR* gene as being causal for omental fat pad mass (20). The C3aR$^{-/-}$ mice were shown to have decreased adiposity as compared with wild-type mice on a regular diet (20). Monocytes and macrophages express the C3aR (21–28). Increased C3a levels also correlate with obesity, diabetes, cholesterol, and lipid levels (29–34). We therefore sought to investigate the specific role of the C3aR in insulin resistance, obesity, and macrophage function utilizing both normal diet and the diet-induced obesity model.

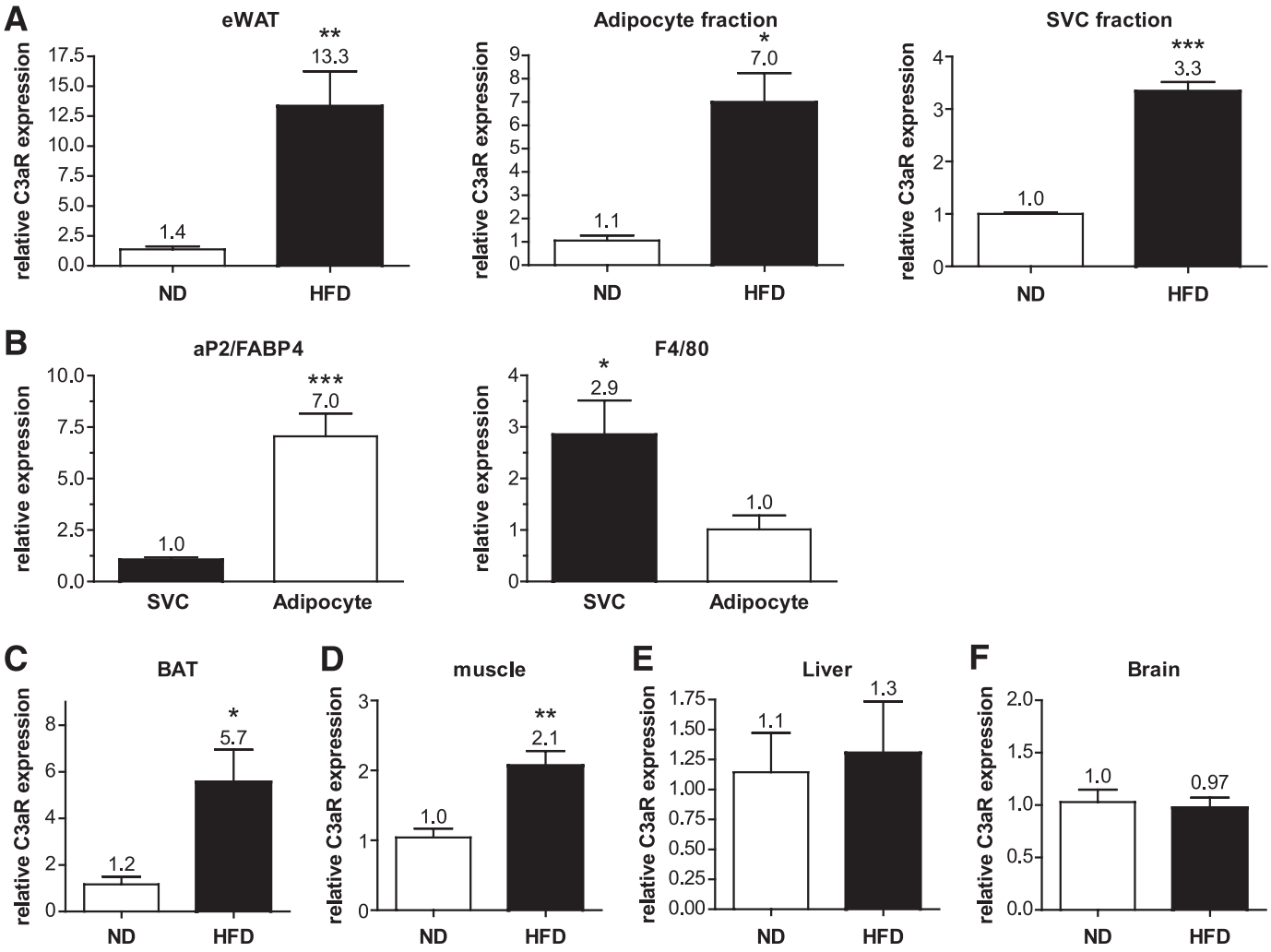

FIG. 1. C3aR mRNA expression is modulated by an HFD. Total RNA was extracted from various tissues from lean (n = 10) and obese (n = 10, 8–16 weeks on HFD) mice. *A*: Total eWAT, adipocyte-purified fraction, and the SVC fraction. *B*: Quantitative PCR on aP2/FABP4 (adipocyte marker) and F4/80 (macrophage marker) confirmed the proper isolation of each fraction. *C*: BAT. *D*: Muscle. *E*: Liver. *F*: Brain. mRNA expression was examined by quantitative RT-PCR (Taqman) and normalized to cyclophilin B expression. Each PCR was performed in duplicate. The following probes from Applied Biosystems were used: cyclophilin B, Mm00478295_m1; F4/80, Mm00802530_m1; CD68, Mm00839636_g1; and C3aR, Mm02620006_s1 and Mm01184110_m1. *P < 0.05; **P < 0.01; ***P < 0.001 by unpaired t test.

RESEARCH DESIGN AND METHODS

C3aR$^{-/-}$ mice generation, genotyping, and treatments. The C3aR$^{-/-}$ C57BL6 mice were generated by Deltagen (San Mateo, CA). The knockout and heterozygous mice are in a pure C57BL6 background (backcrossed seven times). All animals used in the studies were males, age matched (5–7 weeks old, unless mentioned otherwise), and normalized for body weight. Mice were fed either a normal diet (Teklad Global 2018; Harlan Teklad) composed of 6% fat Kcal or high-fat diet (HFD) (D12492; Research Diet) composed of 60% fat Kcal.

Measurements of plasma lipids, insulin, leptin, free fatty acids, ketones, liver enzymes, and quantitative nuclear magnetic resonance. Whole-blood insulin was measured using an insulin enzyme-linked immunosorbent assay kit (Crystal Chem), according to the manufacturer's protocol. Free fatty acids (FFAs) and ketones were assessed from EDTA plasma using the FFA Colorimetric Test and the Autokit Total Ketone Bodies (Wako Diagnostics). Lipid profile and liver enzymes were measured using an automated Vitros analyzer. Lean and fat content was determined by Echo3in1 quantitative nuclear magnetic resonance (qNMR) (EchoMedical Systems).

Histology and immunohistochemistry of adipose tissue and liver. Routing Mayer's heamatoxylin and eosin staining was performed on white adipose tissue (WAT) and liver sections (5 μm) from all studied animals. F4/80 immunohistochemistry (IHC) was performed as described in ref. 8.

Liver triglyceride assay. Frozen liver (~50 mg) samples were homogenized in 1 ml of methanol by magnalyser homogenization (6,500 rpm × 30 s; Roche). Lipids were extracted as described in ref. 35. Triglyceride levels were assessed using a serum triglyceride kit (no. TR0100-1KT; Sigma).

Western blot analysis. Tissue whole-cell extracts were obtained by magnalyser homogenization (Roche). A total of 100 mg of liver/muscle and 200 mg of WAT were homogenized in 500 μl of CHAPS lysis buffer. Antibodies were from the following sources and used at a 1:1,000 dilution: α-AKT and α-AKT ser473 from Cell Signaling, α-insulin receptor (IR) from Santa Cruz, α-IR Tyr1162/1163/1158 from Biosource, and α-CD68 from AbD Serotec. Fujifilm Multi-Gauge V3 software was used for quantification.

Adipose tissue fractionation. Equal amounts of epididymal WAT (eWAT) were collected from mice. Tissue fractionation was performed as described in ref. 8.

RNA extraction and quantitative PCR. RNA from tissues and fractions of pelleted cells was extracted using an RNeasy lipid mini kit (Qiagen). RNA (1 μg) was reverse transcribed using a Taqman reverse transcription reagent kit (Applied Biosystem). Control RT reactions were also performed to assess genomic DNA contamination. Quantitative real-time PCR was performed with 50 ng of the cDNA per reaction using the Taqman Fast Universal PCR Master Mix (Applied Biosystem) on a 7900HT Fast Real-Time PCR System.

Macrophage isolation, polarization, and cytokine analysis. Bone marrow cells were collected from femurs of five lean wild-type, C3aR$^{+/-}$, and C3aR$^{-/-}$ mice (6–7 weeks old) (14). Thioglycollate-elicited peritoneal macrophage isolation was performed as described in ref. 28. Polarization was performed as described in ref. 14. Cytokine expression from 30 ul of EDTA mouse plasma and cell supernatants was measured using the MesoScale Discovery systems. Both multiplex (interleukin [IL]-1β, IL-2, IL-4, IL-6, IL-10, monocyte chemoattractant protein [MCP]-1, KC/GRO, tumor necrosis factor-α, RANTES, and

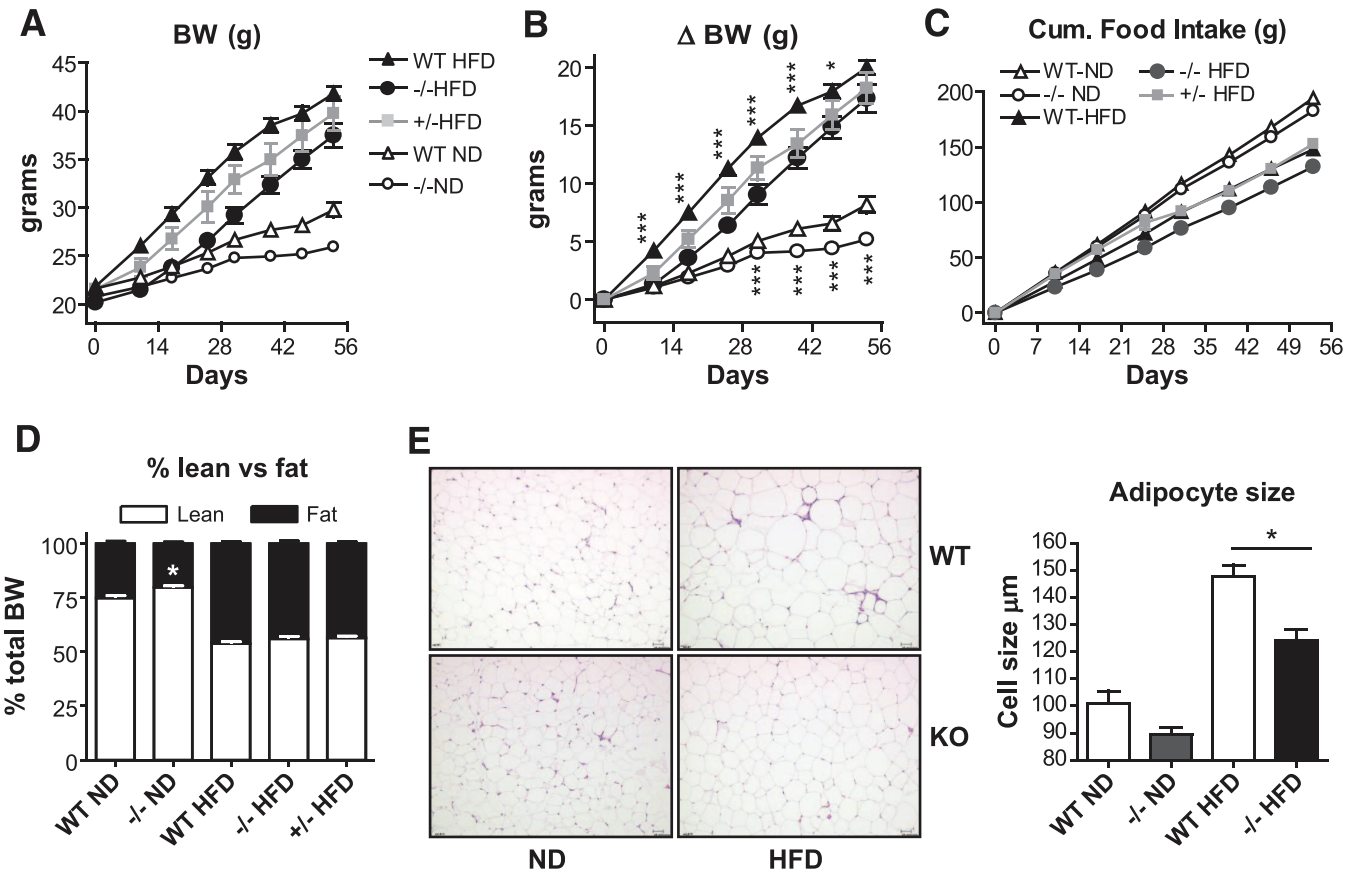

FIG. 2. The effect of C3aR deficiency on diet-induced obesity. The cohorts of C3aR$^{-/-}$, C3aR$^{+/-}$, and wild-type (WT) mice were initially age and weight matched. *A*: Absolute body weight in grams over the 8-week period. *B*: Difference (Δ) in body weight gain in grams. *C*: Food intake in grams. *D*: qNMR analysis of whole-body fat and lean tissue content expressed as a percent of total body weight was performed at 7 weeks of HFD. Data for *A–C* are presented as means ± SE (n = 8–12 per group, except n = 4 for $^{+/-}$). *E*: eWAT sections stained with hematoxylin and eosin with adipocyte cell size measured by light microscopy (three sections per mice; n = 6 per group). *P < 0.05; **P < 0.01; ***P < 0.001 by ANOVA. (A high-quality digital representation of this figure is available in the online issue.)

GM-CSF) and single plex (IL-12p40, interferon-γ) plates were used with the SI6000 plate reader. Samples were run in triplicate.

RESULTS

C3aR expression in tissues. The functions of both C3a and the C3aR have been primarily investigated in the context of an immune response; thus, analyses of complement components have focused largely on organs and cells of the immune system. We therefore investigated C3aR mRNA expression in a broad spectrum of tissues from C57BL6 mice (see Fig. S1 in the online appendix [available at http://diabetes.diabetesjournals.org/cgi/content/full/db09-0323/DC1]). Literature suggests that C3a levels correlate with obesity (31); we therefore investigated the expression of the C3aR in C57BL6 mice after HFD. Interestingly, C3aR mRNA expression was increased 13-fold in the eWAT from mice on HFD (Fig. 1*A*). Subfractionation of the eWAT into adipocyte fraction and stromal vascular cell (SVC) fraction (mainly macrophages and preadipocytes) revealed that C3aR expression was significantly overexpressed in both fractions (Fig. 1*A*). Quantitative RT-PCR for aP2/FABP4 (adipocyte marker) and F4/80 (macrophage marker) confirmed the proper isolation of each fraction (Fig. 1*B*). C3aR expression was significantly increased in brown adipose tissue (BAT) (sixfold) (Fig. 1*C*). A slight increase in C3aR expression was also seen in muscle (twofold) (Fig. 1*D*). No increase in C3aR expression was seen in the liver, brain, or pancreas of mice on HFD (Fig. 1*E* and *F*) (data not shown). A striking note is that the expression level of C3aR mRNA was significantly higher in adipose tissue (total and fractions) compared with all other tissues (online appendix Fig. S2). C3aR expression was also assessed in mouse 3T3-L1 adipocytes and several macrophage cell lines. Significantly higher C3aR expression was detected in the macrophage cell lines (online appendix Fig. S8). We have also shown that C3aR mRNA is very highly expressed in Kupffer cells while present in low levels in hepatocytes and total liver (data not shown). Interestingly, C3aR expression in both these cell types did not vary after HFD (data not shown) unlike C3aR expression in the adipocyte and SVC fractions (Fig. 1*A*). These data suggest that C3aR expression is high in adipose tissue, particularly in the macrophage-containing fraction, increases during HFD, and may play an important role in adipose tissue function.

The effect of C3aR deficiency on diet-induced obesity. To investigate the role of C3aR in insulin resistance and obesity, a deletion of mouse *C3aR* was generated by the insertion of a LacZ-neo cassette (online appendix Fig. S3a). PCR confirmed the proper disruption of the *C3aR* gene (online appendix Fig. S3b). C3aR$^{-/-}$ mice generated were normal, fertile, and showed no significant pathophysiological defect (data not shown) (Deltagen). Quantitative RT-PCR confirmed the absence of C3aR mRNA in tissues of C3aR$^{-/-}$ compared with wild-type mice (data not shown). As expected, heterozygous mice also had a signif-

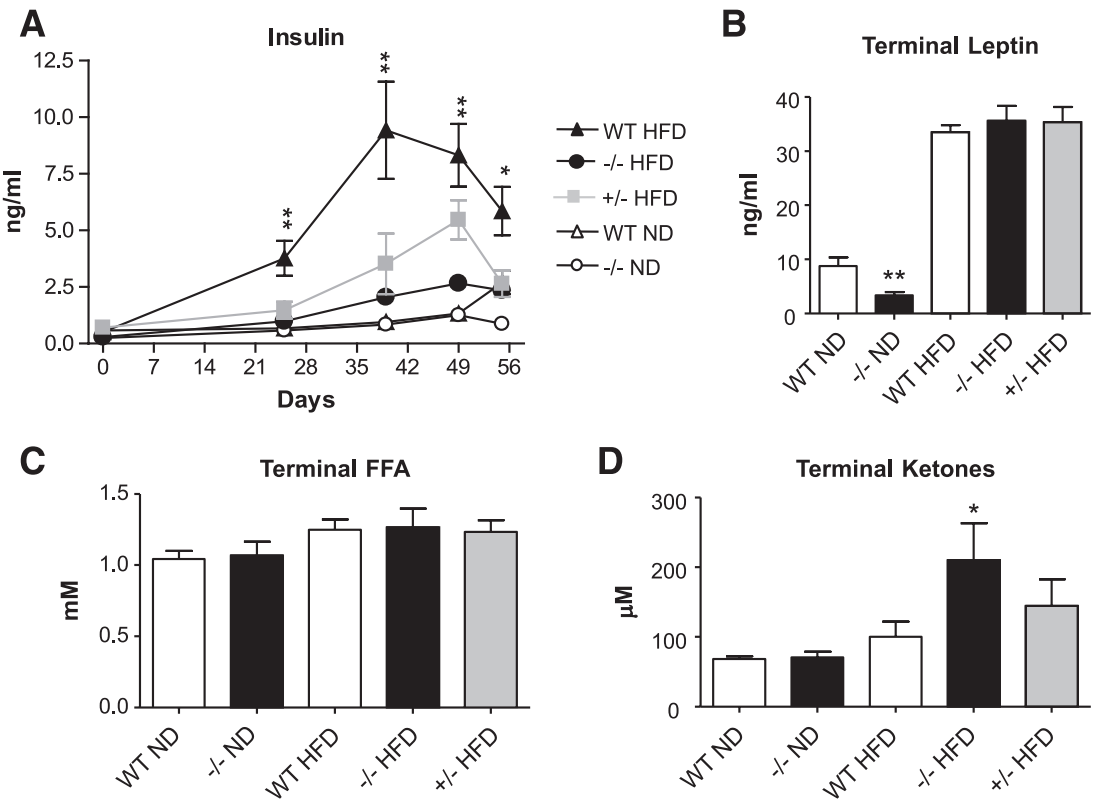

FIG. 3. Metabolic profile of C3aR$^{-/-}$ mice after 8 weeks on an HFD. *A*: Whole-blood insulin over an 8-week period. *B*: Terminal plasma leptin. *C*: Terminal plasma FFAs. *D*: Terminal plasma ketones measured. Data are presented as means ± SE (n = 8–12 per group, except n = 4 for $^{+/-}$). Measurement performed in triplicate. *P < 0.05; **P < 0.01 by ANOVA.

icant decrease (~50%) in C3aR mRNA levels (online appendix Fig. S3c).

To investigate the role of the C3aR in insulin resistance and obesity, knockout mice were put on an 8-week HFD. Initially, the body weight of C3aR$^{-/-}$ and C3aR$^{+/-}$ mice at 5 weeks of age was not significantly different compared with the wild-type controls (Fig. 2*A* and *B*). The C3aR$^{-/-}$ mice gained on average 4–6 g (10–13%) less weight than the wild-type mice during the first 4 weeks of the study. The C3aR$^{+/-}$ mice also showed an intermediate weight-gain phenotype (2–3 g less than wild type) (Fig. 2*A* and *B*). The resistance to weight gain observed in the C3aR$^{-/-}$ mice was more pronounced early in the study and reduced to 3% by 7 weeks on HFD. Terminal weights were equivalent in all groups after 8 weeks on HFD (Fig. 2*A* and *B*). Three independent diabetes-induced obesity studies confirmed the early resistance to weight gain, which attenuated over time (online appendix Fig. S7 and data not shown). Cumulative food intake on HFD was only slightly decreased in the C3aR$^{-/-}$ compared with wild type (Fig. 2*C*). Other diabetes-induced obesity studies showed no effect on food intake (online appendix Fig. S7 and data not shown). To examine the effects on total fat depots and lean mass, qNMR was performed. In contrast to normal-diet (ND)-fed C3aR$^{-/-}$ mice, which had a decreased fat-to-lean ratio, the C3aR$^{-/-}$ mice on HFD were not discriminated from their wild-type counterparts (Fig. 2*D*). The qNMR results reinforce the phenotype seen in C3aR$^{-/-}$, where terminal weights on HFD were equivalent to wild type (Fig. 2*A* and *B*). Furthermore, no significant difference in subcutaneous versus abdominal fat mass was observed for all mice on HFD (data not shown). Adipose tissue histology revealed a decrease in adipocyte size in the C3aR$^{-/-}$ compared with wild type on both diets (Fig. 2*E*). Interestingly, the C3aR$^{-/-}$ mice on a ND gained less weight (1–3 g less) over time compared with wild type (Fig. 2*A* and *B*). In summary, C3aR$^{-/-}$ mice were initially resistant to body weight gain on HFD, but this resistance was transient and lost over time. This resistance is also more significant when mice are maintained on regular diet.

Metabolic profile of C3aR$^{-/-}$ mice on HFD. To further understand the phenotypic changes in the C3aR$^{-/-}$ mice, several metabolic end points were investigated in lean and obese C3aR$^{-/-}$ mice. Over the 8-week time course, blood insulin levels were monitored. Between days 25 and 55, the wild-type mice on HFD had between a two- and fivefold increase in insulin excursion compared with the C3aR$^{-/-}$ mice (Fig. 3*A*). In fact, insulin levels in the C3aR$^{-/-}$ mice on HFD were normalized to wild-type mice on a regular diet. The heterozygous mice on HFD also showed a decreased insulin excursion, which was intermediate between the wild-type and C3aR$^{-/-}$ mice (Fig. 3*A*). Terminal leptin and FFA levels were not significantly altered in the different groups on HFD (Fig. 3*B* and *C*). A significant decrease in leptin was observed in C3aR$^{-/-}$ mice on regular diet compared with wild-type mice (Fig. 3*B*), consistent with a decreased adiposity (Fig. 2*D*) (20). No such effect on leptin was seen in all mice on HFD consistent with the equivalent terminal body weights (Fig. 2*A*–*C*). An increase in terminal ketone bodies on HFD was detected in the C3aR$^{-/-}$ mice (Fig. 3*D*). An effect on fatty acid oxidation is unlikely in the C3aR$^{-/-}$ mice; no corresponding effect on terminal FFA levels was observed (Fig. 3*C*) in conjunction with the significant variation in the ketone bodies measurement seen within each group on HFD (Fig. 3*E*). Given the decreased insulin excursion in

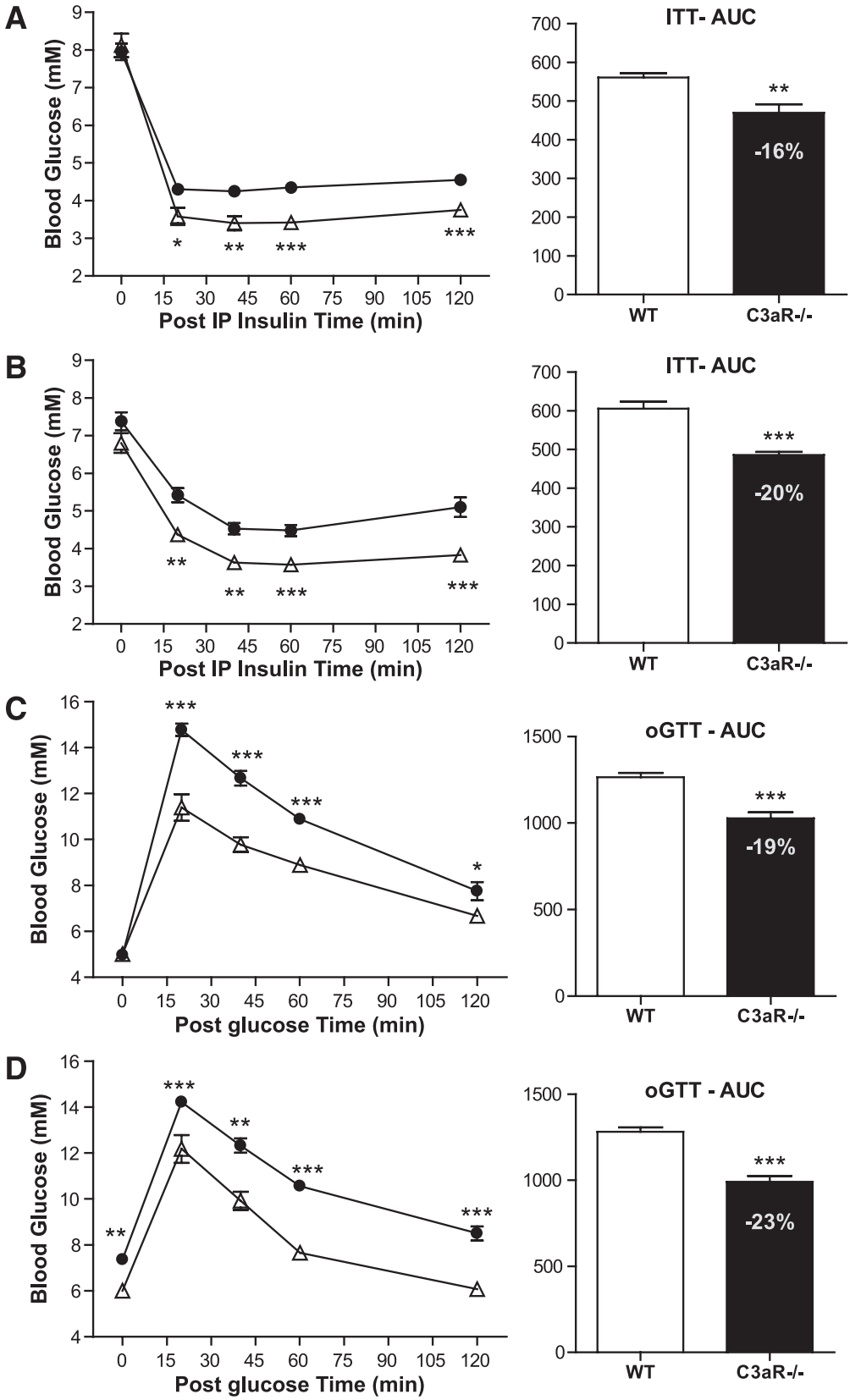

FIG. 4. ITT and OGTT in C3aR$^{-/-}$ mice. Nine-week-old wild-type (WT) and C3aR$^{-/-}$ males (n = 6 per group) for ITT on ND (*A*) and on an 8-week HFD (*B*) were starved for 4 h and injected with one dose of insulin (0.3 units/kg i.p.). *A*: ●, wild type; △, C3aR1$^{-/-}$ ND. *B*: ●, wild type HFD; △, C3aR$^{-/-}$ HFD. For OGTT, mice were starved for 24 h and then administered one dose of glucose (2 g/kg p.o.) on 2 weeks HFD (*C*) and on 8 weeks HFD (*D*). *C*: ●, wild type; △, C3aR$^{-/-}$. *D*: ●, wild type HFD; △, C3aR$^{-/-}$ HFD. Blood glucose was measured from tail vein after 0, 20, 40, 60, and 120 min. AUC was calculated. *P < 0.05; **P < 0.01; ***P < 0.001 by ANOVA.

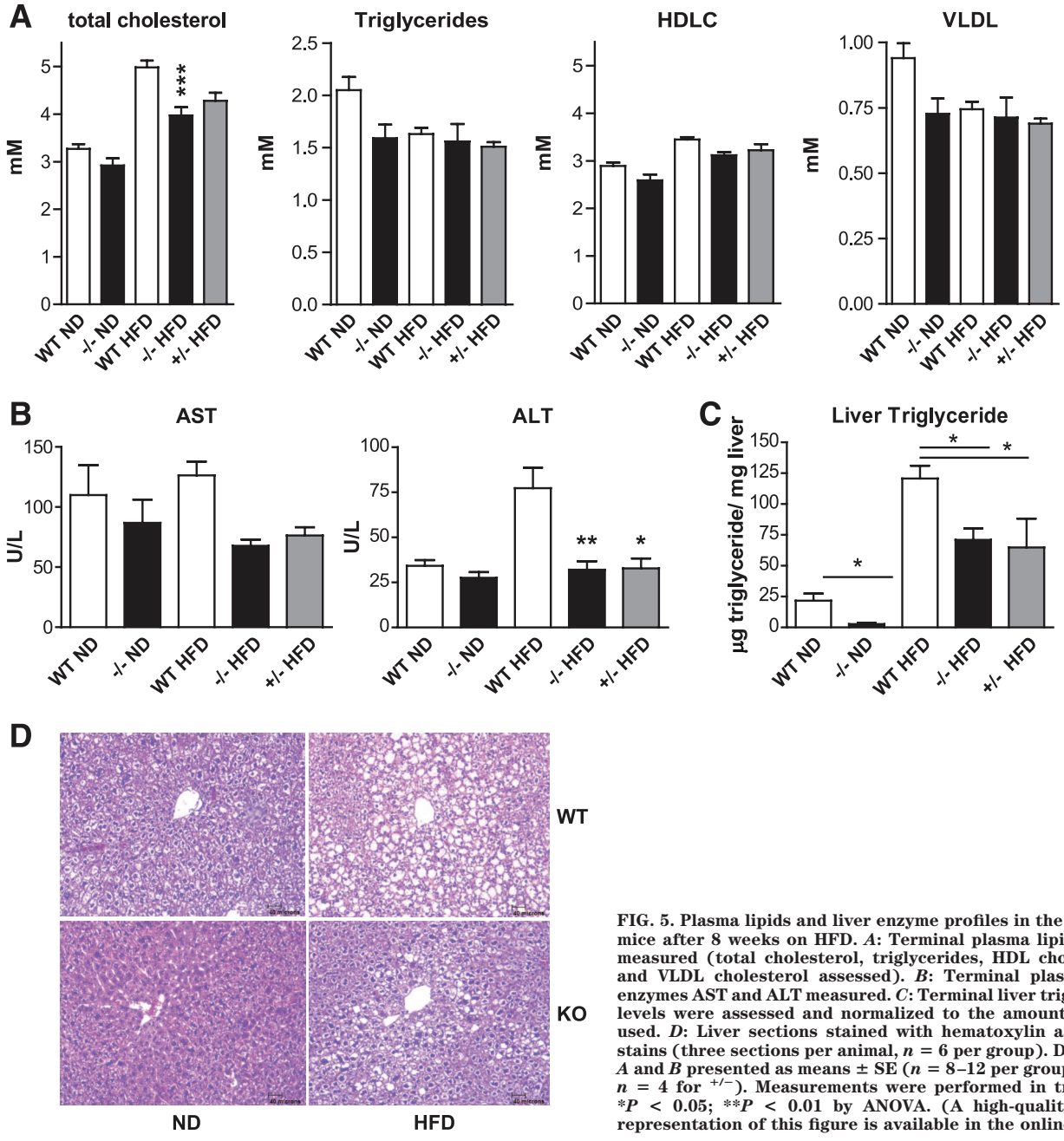

FIG. 5. Plasma lipids and liver enzyme profiles in the C3aR$^{-/-}$ mice after 8 weeks on HFD. *A*: Terminal plasma lipid profile measured (total cholesterol, triglycerides, HDL cholesterol, and VLDL cholesterol assessed). *B*: Terminal plasma liver enzymes AST and ALT measured. *C*: Terminal liver triglyceride levels were assessed and normalized to the amount of liver used. *D*: Liver sections stained with hematoxylin and eosin stains (three sections per animal, $n = 6$ per group). Data from *A* and *B* presented as means ± SE ($n = 8$–12 per group, except $n = 4$ for $^{+/-}$). Measurements were performed in triplicate. *$P < 0.05$; **$P < 0.01$ by ANOVA. (A high-quality digital representation of this figure is available in the online issue.)

the C3aR$^{-/-}$ mice during HFD (Fig. 3*A*), we performed an insulin tolerance test (ITT) in order to clearly assess insulin sensitivity (Fig. 4*A* and *B*). A significant decrease in blood glucose during the ITT was seen in the C3aR$^{-/-}$ mice on ND and HFD compared with wild-type mice. An overall decrease in 16 and 20% blood glucose area under the curve was seen in the C3aR$^{-/-}$ mice (Fig. 4*A* and *B*). An oral glucose tolerance test (OGTT) also resulted in a significant decrease in blood glucose excursion in the C3aR$^{-/-}$ mice (Fig. 4*C* and *D*). The decreased insulin excursion on HFD (Fig. 3*A*) and the decreased glucose excursion (Fig. 4) clearly demonstrate that the C3aR$^{-/-}$ mice are more insulin sensitive.

Several lipid parameters were also analyzed; a decrease in total cholesterol was detected in the C3aR$^{-/-}$ mice on HFD (Fig. 5*A*). No effect on triglycerides, HDL cholesterol, or VLDL cholesterol was detectable (Fig. 5*A*). Plasma liver enzymes aspartate transaminase and alanine transaminase were also decreased in both the C3aR$^{-/-}$ and C3aR$^{+/-}$ mice on HFD (Fig. 5*B*). Liver triglyceride levels were also measured; C3aR$^{-/-}$ on both ND and HFD had a significant reduction in liver triglyceride levels compared with wild type (Fig. 5*C*). The C3aR$^{+/-}$ mice also showed a significant decrease in liver triglycerides on HFD (Fig. 5*C*). Liver histology confirmed that the C3aR$^{-/-}$ mice on both ND and HFD had significantly less lipid accumulation compared with wild type (Fig. 5*D*). Both decreased liver enzymes and liver triglycerides suggest decreased liver steatosis. Overall, profiling of C3aR$^{-/-}$ mice suggests that they are protected from HFD-induced insulin resistance as seen by both metabolic profiling and increased insulin sensitivity. Furthermore, these mice are also protected from HFD-induced liver steatosis.

Insulin sensitivity of key metabolic tissues. To determine which tissues contributed to the increased insulin sensitivity, we performed an acute in vivo insulin chal-

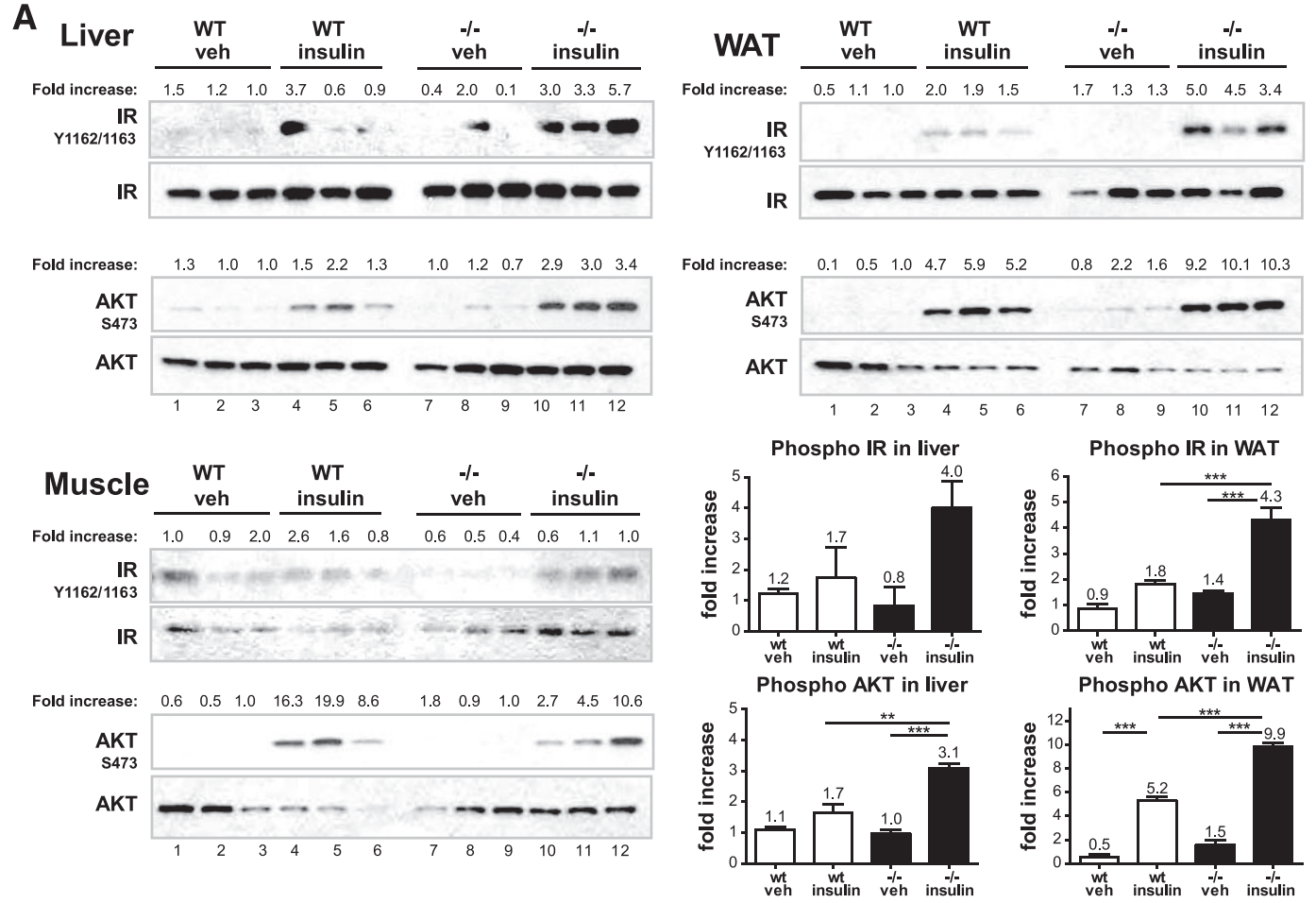

FIG. 6. Acute insulin challenge in C3aR$^{-/-}$ mice. Wild-type (WT) and C3aR$^{-/-}$ mice (5–6 weeks old) on ND (*A*) and HFD (6 weeks) (*B*) were starved for 6 h (n = 6 per group) and injected with one dose of insulin (0.3 units/kg i.p.) or vehicle. Five minutes postinjection, tissues were collected (liver, skeletal muscle [gastrocnemius], and eWAT). Tissues were homogenized and protein extracted and analyzed by SDS-PAGE. Nitrocellulose membranes were probed with antibodies: α-IR β-chain, α-IR β-chain phosphoTyr1162/Tyr1163, α-AKT, and α-AKT phosphoSer473. Each lane represents tissue protein extract from one individual animal. Fold increase is calculated by dividing the signal intensity of the phosphorylated protein by the signal intensity of the total protein. Fold changes in protein phosphorylation were graphed. *P < 0.05; **P < 0.01; ***P < 0.001 by ANOVA.

lenge and profiled key metabolic tissues (liver, WAT, and muscle) on ND (Fig. 6*A*) and HFD (Fig. 6*B*). Both wild-type and C3aR$^{-/-}$ mice (5–6 weeks old) were starved for 6 h, after which a single dose of insulin was administered in the peritoneum. Tissues were collected 5 min postdose, and IR signaling was examined. Interestingly, an increased IRβ chain and AKT phosphorylation and thus activation was seen in both the liver and eWAT of lean C3aR$^{-/-}$ mice upon challenge compared with wild type (2- to 2.5-fold increase) (Fig. 6*A*, *lanes 10–12* compared with *lanes 4–6*). Furthermore, the eWAT from vehicle-treated C3aR$^{-/-}$ animals also possessed a slightly increased basal AKT phosphorylation (Fig. 6*A*, *lanes 7–9* compared with *lanes 1–3*), also suggesting increased insulin sensitivity. An increased AKT phosphorylation was seen in the liver and eWAT of C3aR$^{-/-}$ mice on HFD upon challenge compared with wild type (5.6- and 2-fold increase) (Fig. 6*B*, *lanes 10–12* compared with *lanes 4–6*). Increased IRβ chain phosphorylation was more evident in WAT (2.5-fold) (Fig. 6*B*, *lanes 10–12* compared with *lanes 4–6*). The C3aR$^{+/-}$ mice showed an intermediate phenotype (Fig. 6*B*, *lanes 13–15*). No significant change in IR signaling was seen in muscle (Fig. 6*A* and *B*). In all, these results suggest that C3aR$^{-/-}$ mice are more insulin sensitive, both biochemically and as demonstrated by the ITT and OGTT challenges (Figs. 4 and 6).

Macrophage infiltration in adipose tissue. Several recent studies (4–7) have demonstrated an important role for adipose tissue macrophages (ATMs) in mediating insulin resistance during obesity. These studies have shown that macrophages can be polarized to two states (36). Interestingly, M1 macrophages (classical proinflammatory) have been shown to increase in the obese insulin-resistant adipose tissue, while M2 (alternative anti-inflammatory) are mostly present in lean insulin-sensitive WAT (4–8,36). We therefore investigated the function of macrophages in the C3aR$^{-/-}$ mice. Macrophage infiltration in the adipose tissue was assessed by quantifying the levels of two macrophage markers (F4/80 and CD68) (37). Staining of adipose tissue sections with an anti-F4/80 antibody revealed a significant decrease in macrophage infiltration in WAT from C3aR$^{-/-}$ mice on HFD (Fig. 7*A*). Typical crown-like structures (several macrophages surrounding an adipocyte) usually present in obese insulin-resistant WAT (8) were virtually absent in C3aR$^{-/-}$ adipose tissue after 8 weeks of HFD (Fig. 7*A*). Analysis of WAT proteins by immunoblot with CD68-specific antibodies confirmed the results seen by the F4/80 IHC. As

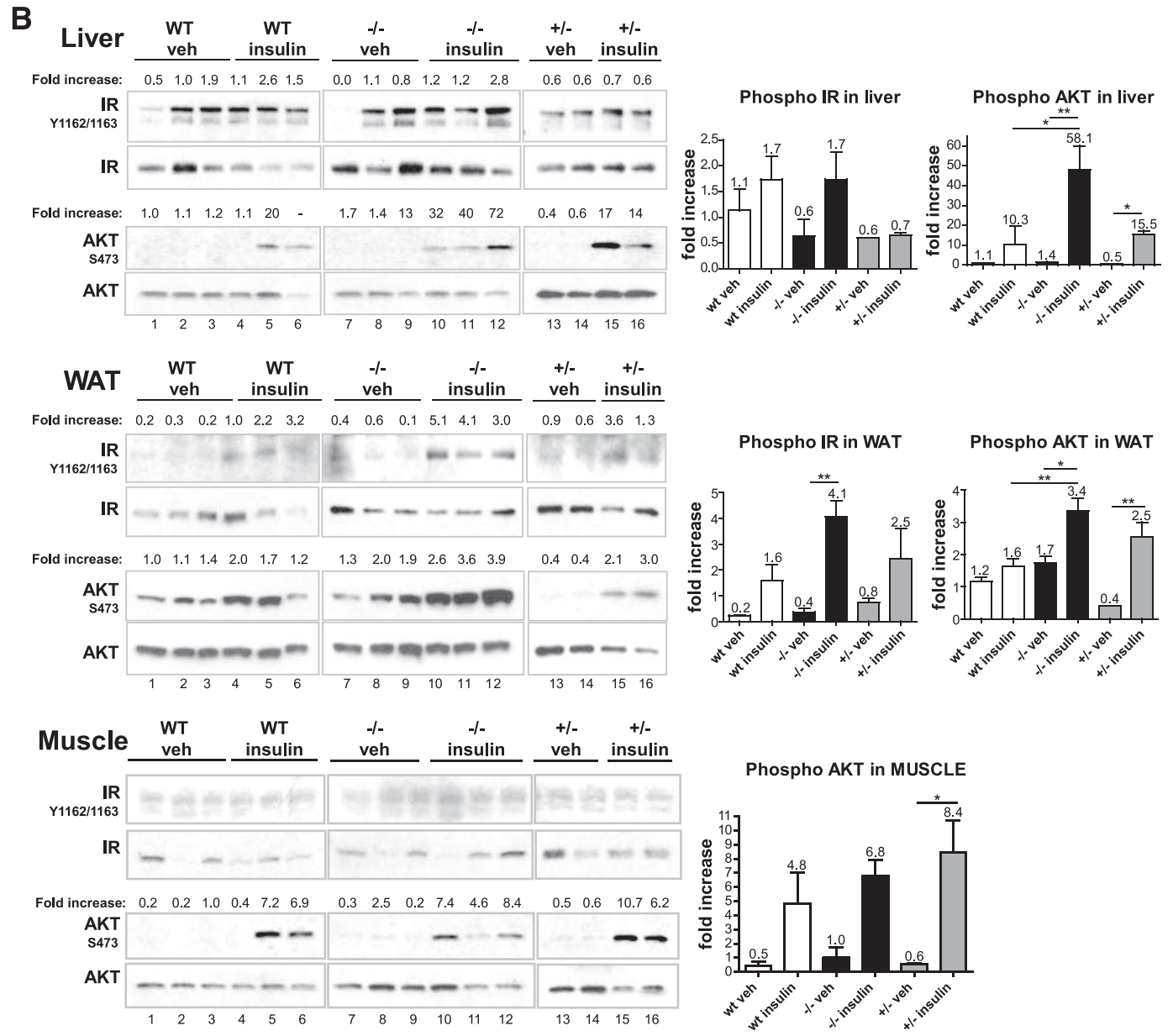

FIG. 6. Continued.

expected, a significant increase in CD68 protein levels was seen in wild-type mice on HFD compared with ND (six-fold) (Fig. 7*B*, *lanes 7–9* compared with *lanes 1–3*). Interestingly, CD68 protein expression was significantly lower in eWAT from C3aR$^{-/-}$ or C3aR$^{+/-}$ on HFD as compared with wild-type HFD (2- and 2.7-fold decrease) (Fig. 7*B*, *lanes 10–14* compared with *lanes 1–3*); CD68 levels in C3aR$^{-/-}$ mice on HFD were similar to those seen in mice on ND (Fig. 7*B*, *lanes 10–14* compared with *lanes 1–6*). Liver CD68 expression was unchanged after HFD in all mice (data not shown). Quantitative PCR analysis of CD68 and F4/80 mRNA expression (Fig. 7*C*) confirmed the CD68 immunoblot and F4/80 IHC results.

We also investigated the expression pattern of M1- and M2-specific genes within the adipose tissue: MCP-1 and IL-6 are adipokines believed to initiate macrophage infiltration in the WAT and involved in systemic insulin resistance (rev. in 5,18). Indeed, a significant increase in MCP-1 mRNA levels was seen in wild-type mice on HFD compared with ND (fourfold) (Fig. 7*D*). MCP-1 expression in C3aR$^{-/-}$ mice on HFD was 1.7-fold lower than wild-type controls. Interestingly, C3aR$^{-/-}$ on ND also had a 1.8-fold lower MCP-1 mRNA expression compared with wild type on ND consistent with decreased adiposity (Fig. 7*D*). A definitive trend toward decreased IL-6 expression was seen in both the C3aR$^{-/-}$ and C3aR$^{+/-}$ mice on HFD compared with wild type (Fig. 7*D*). We investigated the expression of M2-specific genes. Arginases are overexpressed in M2 macrophages and believed to be involved in adipose tissue repair (37). Adipose tissue from C3aR$^{-/-}$ mice on ND showed a dramatic increased in Arg2 (Fig. 7*D*). Arg2 levels are also increased in the knockout mice on HFD to a lesser extent than on ND. No change in other M2-specific genes (Arg1, Mrc2, Mgl1, Mgl2, and Ym1) was detected in eWAT (data not shown). We also investigated the expression of several adipogenesis genes (peroxisome proliferator–activated receptor [PPAR]γ, CD36, LPL, DGAT1, and aP2) as well as fatty oxidation genes (uncoupling pro-

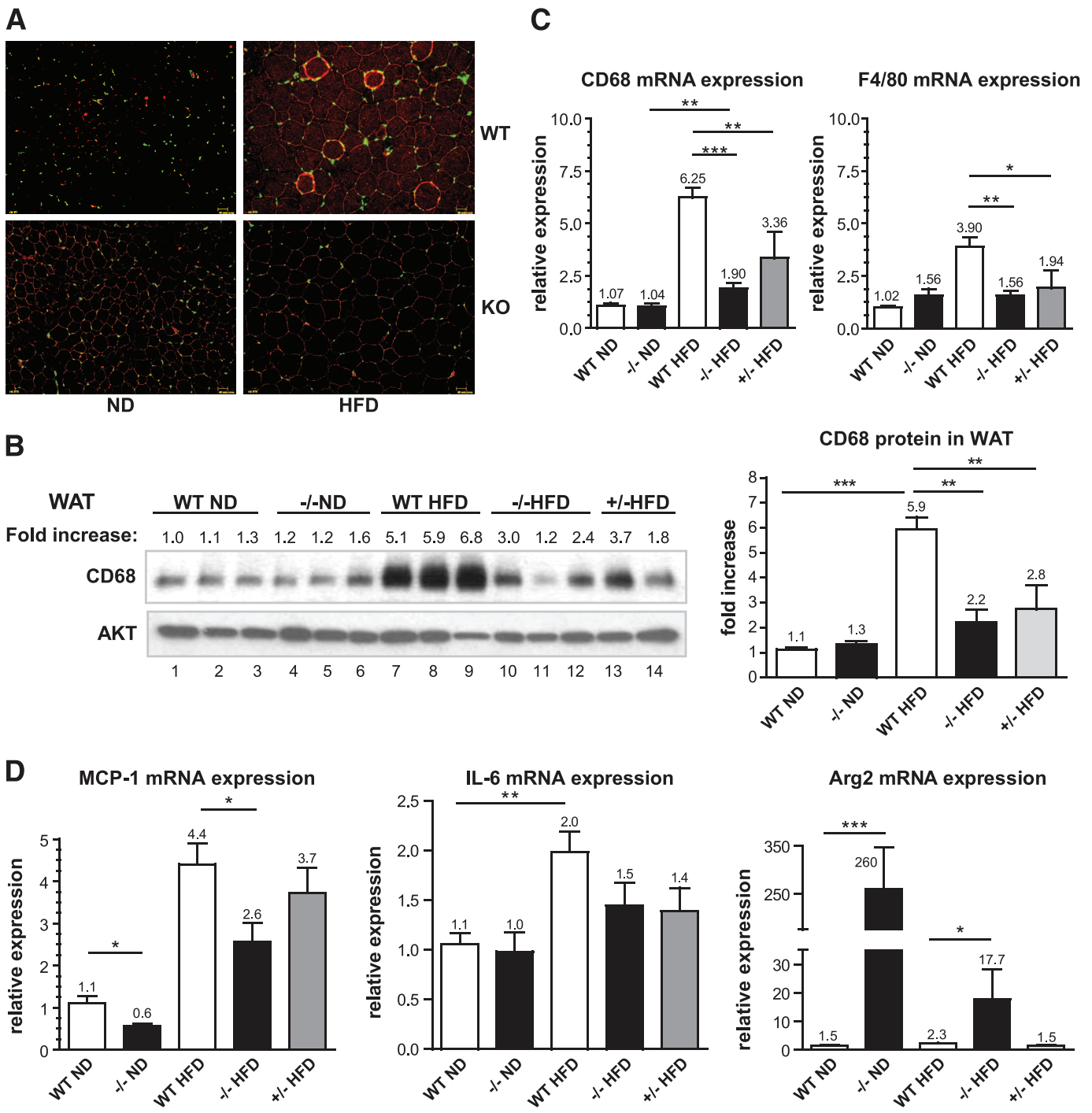

FIG. 7. Macrophage infiltration and gene expression profile in the eWAT after 8 weeks on HFD. *A*: Sections of eWAT (three sections per animals, *n* = 6 per group) were fixed and stained with a α-F4/80 antibody (macrophage marker). Fluorescence microscopy was used to visualize macrophages (red) surrounding adipocytes. Nuclei (green) were stained by DAPI. *B*: Total eWAT was homogenized and proteins extracted and analyzed by SDS-PAGE. Each lane represents eWAT protein extract from one individual animal. Nitrocellulose membranes were probed with α-CD68 (macrophage marker) and α-AKT (loading control) antibodies. Fold increase in CD68 is calculated by dividing the signal intensity of the CD68 protein by the signal intensity of AKT. Fold changes in CD68 protein levels were graphed. RNA was extracted from eWAT and quantitative RT-PCR performed for CD68 and F4/80 (*C*) and MCP-1, IL-6, and Arg2 mRNA expression (*D*). All reactions were done in duplicate. Data presented as means ± SE (*n* = 8–12 per group, except *n* = 4 for $^{+/-}$). All PCR were performed in duplicate. mRNA expression was normalized to cyclophilin B. The following probes from Applied Biosystems were used: cyclophilin B, Mm00478295_m1; F4/80, Mm00802530_m1; CD68, Mm00839636_g1; MCP-1/CCL2, Mm00441242_m1; IL-6, Mm00446190_m1; Arg2, Mm00477592_m1; Arg1, Mm00475988_m1; C3aR, Mm02620006_s1 and Mm01184110_m1. **P* < 0.05; ***P* < 0.01; ****P* < 0.001 by ANOVA. (A high-quality digital representation of this figure is available in the online issue.)

tein-2, PDK2, PDK4, and Acadl) (38) in subcutaneous and abdominal WAT of wild-type and C3aR$^{-/-}$ mice on ND and HFD. No significant difference was observed in the expression of these genes in both fat depots (data not shown). Furthermore, no significant difference in the expression of thermogenesis-related genes, uncoupling protein-1, and PPARγ coactivator-1α in BAT was observed in these mice. Lastly, no significant changes in M1 and M2 gene expression

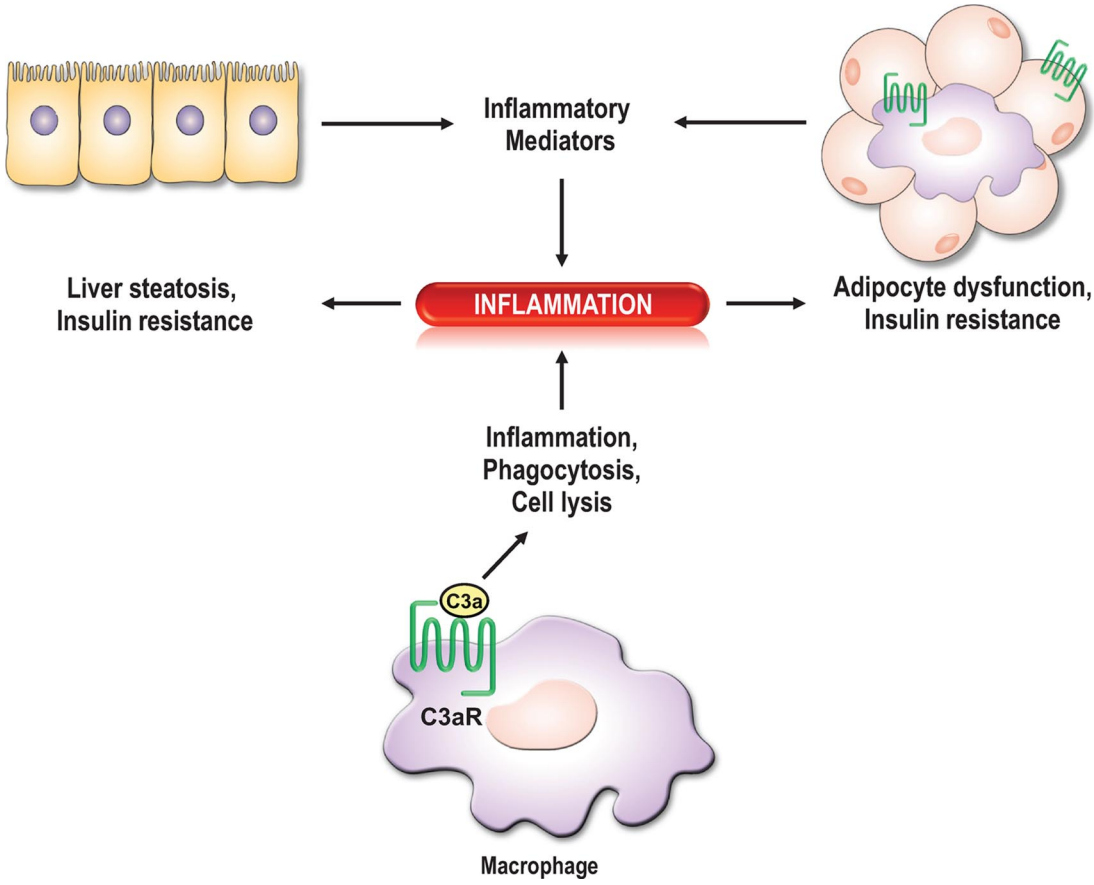

FIG. 8. Model of the role of the C3aR in IR and liver steatosis. Macrophages in the periphery and in tissues (adipose tissue, liver) play an important role in inflammation. Proinflammatory mediators produced by resident macrophages, adipocytes, and hepatocytes stimulate the infiltration of circulating monocytes within the tissue, which differentiate into macrophages. The increased local inflammation affects the insulin responsiveness of the tissue and other organs, thus leading to systemic insulin resistance. The C3aR is highly expressed in both adipocytes and macrophages.

were detected in liver (data not shown). Overall, our data suggest that adipose tissue from C3aR$^{-/-}$ mice has a decreased M1 gene expression profile.

Both local and systemic proinflammatory cytokines have been shown to significantly affect insulin sensitivity of the WAT, liver, and muscle. We therefore examined if the local increase in IL-6 and MCP-1 mRNA expression (Fig. 7*D*) correlated with an increased plasma cytokine expression (online appendix Fig. S4). As expected, a significant increase in proinflammatory cytokines was seen in wild-type mice after 8 weeks of HFD compared with ND (online appendix Fig. S4). Interestingly, no such increase in proinflammatory mediators was seen in the C3aR$^{-/-}$ mice on HFD; the levels were comparable to both wild-type and C3aR$^{-/-}$ mice on ND (online appendix Fig. S4). Consequently, the decreased adipose tissue inflammation (Fig. 7) also translates to a decreased systemic inflammation (online appendix Fig. S4), thus potentially affecting the insulin responsiveness of other tissues.

To understand the role of C3aR in macrophage biology, bone marrow–derived macrophages (BMDMs) from lean wild-type, C3aR$^{-/-}$, and C3aR$^{+/-}$ mice were generated and polarized to M1 and M2. Strikingly, both C3aR$^{+/-}$ and C3aR$^{-/-}$ M1 BMDMs produced considerably fewer proinflammatory cytokines compared with wild type (online appendix Fig. S5a). We further investigated the gene expression pattern of other M1 and M2 genes (online appendix Fig. S5b). Both C3aR$^{+/-}$ and C3aR$^{-/-}$ M1 BMDMs possessed a considerable decreased expression of both Nos1, Nos2, and MARCO (M1 markers) compared with wild type (online appendix Fig. S5b). The expression of several M2 markers (Arg1, Arg2, Mgl1, Mgl2, Ym1, and MRC2) (37) were unchanged (data not shown). Similar results were obtained with thioglycollate-elicited peritoneal macrophages from wild-type and C3aR$^{-/-}$ mice. A significant decrease in M1 markers was seen in the C3aR$^{-/-}$ peritoneal macrophages (online appendix Fig. S6). No effect on M2-specific markers mentioned above was observed (data not shown). Our results demonstrate that C3aR deletion decreases proinflammatory cytokines and M1-specific gene expression in macrophages.

DISCUSSION

Combined genetics, expression analysis, and a systems biology approach using an intercross between several mouse strains were used to identify causal genes involved in tissue adiposity and potential insulin resistance. One of the striking causal genes identified was the C3aR (20). Utilizing knockout mice, we describe a novel role for the C3aR in adipose tissue homeostasis with implications for metabolic syndrome (Fig. 8). This study shows that the C3aR is highly expressed in both adipocytes and macrophages and significantly increases in the WAT after HFD (Figs. 1 and online appendix Fig. S2). C3aR$^{-/-}$ mice were only transiently resistant to body weight gain on HFD (Fig.

2*A–B* and online appendix Fig. S7). The increased leanness phenotype on ND described by Schadt et al. (20) was also recapitulated in this study (Fig. 2). Furthermore, the C3aR$^{-/-}$ mice are protected from HFD-induced insulin resistance and liver steatosis (Fig. 8). Adipose tissue analysis of C3aR$^{-/-}$ mice on HFD revealed a striking decrease in macrophage infiltration with a concomitant reduction in both tissue and plasma proinflammatory cytokine production (Figs. 7 and online appendix Fig. S4). This decreased macrophage infiltration may provide the rationale for decreased adipocyte size seen in C3aR$^{-/-}$ as compared with wild type on HFD. We also show that ATMs, BMDMs, and thioglycollate-elicited peritoneal macrophages express significantly fewer proinflammatory M1 mediators compared with wild type (Figs. 7 and online appendix Figs. S5 and S6). Interestingly, the C3aR$^{-/-}$ mice on ND have significant increased insulin sensitivity (Fig. 4*A*). Our results suggest that C3aR is most likely causal for insulin resistance. This is quite striking and may be indicative of a more pronounced role of macrophages and/or inflammatory genes in insulin resistance.

ATMs have emerged as crucial contributors to both local (tissue-specific) and systemic inflammation (9,19,39,40). In this study, we clearly demonstrate that macrophage infiltration in the adipose tissue is significantly diminished in the C3aR$^{-/-}$ mice on HFD (Fig. 7). Macrophages possess different activation states; shifting the balance from M1 to M2 macrophages in adipose tissue appears to be beneficial to in vivo insulin sensitivity (14,16,17). A clear role of macrophage function in insulin resistance has been demonstrated by the macrophage-specific PPAR$\gamma^{-/-}$ mice (16,17). We also show that macrophage M1 function is significantly diminished in the C3aR$^{-/-}$ ATMs, BMDMs, and thioglycollate-elicited peritoneal macrophages (Figs. 7*D* and online appendix Figs. S5 and S6). Both local (adipose tissue) and systemic inflammation are greatly decreased in the C3aR1$^{-/-}$ mice on HFD (Figs. 7 and online appendix Fig. S4). Overall, the significant decrease in WAT M1 macrophages and their decreased proinflammatory potential may be sufficient to promote insulin sensitivity. Currently, anti-inflammatory agents such as salicylates are being tested in large clinical trials to determine whether they are efficacious in obese diabetic subjects with respect to insulin sensitization (41). Initial data seem to suggest that salicylates can improve glycemia and decrease inflammatory parameters elevated in nondiabetic obese adults (42,43). Thus, targeting inflammation through the modulation of resident macrophage functions may have a significant impact on metabolic disorders.

C3a desArg is a cleavage product of C3a, which acts on a novel receptor, C5L2, to stimulate triglyceride synthesis in the adipose tissue (rev. in 44). The C3$^{-/-}$ mice (the precursor of C3a, C3a desArg, C3b, and iC3b) were generated and showed to have increased FFA as well delayed postprandial clearance of triglycerides on ND and HFDs (45). No significant change in body weight was seen in male C3$^{-/-}$ after 16 weeks on HFD (46). Interestingly, only once the C3$^{-/-}$ were crossed to *ob/ob* mice was significant resistance to body-weight gain observed (47). They also had lower insulin levels and significantly lower homeostasis model assessment index, which was related to their decreased body weight. Therefore, a more pronounced body-weight phenotype in C3aR$^{-/-}$ mice may manifest itself in a leptin-deficient background. Strikingly, we show that the C3aR$^{-/-}$ mice on ND have a consistent resistance to adiposity, and this may explain their increased insulin sensitivity. The role of C3, C3a desArg, and our data on the C3aR provide a clear role of the complement system in negatively impacting adiposity and insulin sensitivity.

With the growing worldwide epidemic in both diabetes and obesity, demands for new therapies are increasing. The complexities of these diseases, which involve multiple organs, add to the difficult task of developing new treatments. Understanding the biology and identifying new druggable targets is a major effort within the pharmaceutical industry. Advances in genomics have helped in identifying potential key drivers of complex traits involved in these diseases (20). The field of insulin resistance and inflammation is still in its infancy. Development of novel therapeutics which interfere with key causal nodes such as the complement pathway may provide a critical link between inflammation and insulin resistance.

ACKNOWLEDGMENTS

The authors are employees of Merck & Co. The nature of our activity is involvement in basic research (biology, pharmacology, and chemistry). The financial arrangement entails a yearly salary as well as stock options. The business purpose of Merck & Co is to discover and develop new therapeutic drugs for the treatment of human diseases. W.T. is an employee of Deltagen. The financial arrangement entails a yearly salary a well as stock options. The business purpose of Deltagen is to develop and distribute transgenic mice lines. No other potential conflicts of interest relevant to this article were reported.

We thank Deltagen for the permission to publish part of their data on the C3aR$^{-/-}$ mice. We also thank D. Ethier and K. Ng for genotyping the C3aR knockout mice; D. Normandin, M. Meilleur, and E. Daigneault for bone marrow cell isolation; and K. Clark for figure design. We acknowledge F. Gervais, A. Therien, J. Mudgett, and R. Askew for providing comments on the manuscript and scientific insight.

REFERENCES

1. Carroll MC. The complement system in regulation of adaptive immunity. Nat Immunol 2004;5:981–986
2. Szebeni J. *The Complement System: Novel Roles in Health and Disease*. Kluwer Academic Publishers, 2004
3. Markiewski MM, Lambris JD. The role of complement in inflammatory diseases from behind the scenes into the spotlight. Am J Pathol 2007;171:715–727
4. de Luca C, Olefsky JM. Inflammation and insulin resistance. FEBS Lett 2008;582:97–105
5. Ferrante AW Jr. Obesity-induced inflammation: a metabolic dialogue in the language of inflammation. J Intern Med 2007;262:408–414
6. Hotamisligil GS. Inflammation and metabolic disorders. Nature 2006;444:860–867
7. Schenk S, Saberi M, Olefsky JM. Insulin sensitivity: modulation by nutrients and inflammation. J Clin Invest 2008;118:2992–3002
8. Lumeng CN, Bodzin JL, Saltiel AR. Obesity induces a phenotypic switch in adipose tissue macrophage polarization. J Clin Invest 2007;117:175–184
9. Weisberg SP, McCann D, Desai M, Rosenbaum M, Leibel RL, Ferrante AW Jr. Obesity is associated with macrophage accumulation in adipose tissue. J Clin Invest 2003;112:1796–1808
10. Arkan MC, Hevener AL, Greten FR, Maeda S, Li ZW, Long JM, Wynshaw-Boris A, Poli G, Olefsky J, Karin M. IKK-beta links inflammation to obesity-induced insulin resistance. Nat Med 2005;11:191–198
11. Solinas G, Vilcu C, Neels JG, Bandyopadhyay GK, Luo JL, Naugler W, Grivennikov S, Wynshaw-Boris A, Scadeng M, Olefsky JM, Karin M. JNK1 in hematopoietically derived cells contributes to diet-induced inflammation and insulin resistance without affecting obesity. Cell Metab 2007;6:386–397
12. De Taeye BM, Novitskaya T, McGuinness OP, Gleaves L, Medda M,

Covington JW, Vaughan DE. Macrophage TNF-alpha contributes to insulin resistance and hepatic steatosis in diet-induced obesity. Am J Physiol Endocrinol Metab 2007;293:E713–E725
13. Kang K, Reilly SM, Karabacak V, Gangl MR, Fitzgerald K, Hatano B, Lee CH. Adipocyte-derived Th2 cytokines and myeloid PPARdelta regulate macrophage polarization and insulin sensitivity. Cell Metab 2008;7:485–495
14. Odegaard JI, Ricardo-Gonzalez RR, Red EA, Vats D, Morel CR, Goforth MH, Subramanian V, Mukundan L, Ferrante AW, Chawla A. Alternative M2 activation of Kupffer cells by PPARdelta ameliorates obesity-induced insulin resistance. Cell Metab 2008;7:496–507
15. Charo IF. Macrophage polarization and insulin resistance: PPAR gamma in control. Cell Metabolism 2007;6:96–98
16. Odegaard JI, Ricardo-Gonzalez RR, Goforth MH, Morel CR, Subramanian V, Mukundan L, Eagle AR, Vats D, Brombacher F, Ferrante AW, Chawla A. Macrophage-specific PPARgamma controls alternative activation and improves insulin resistance. Nature 2007;447:1116–1120
17. Bouhlel MA, Derudas B, Rigamonti E, Dievart R, Brozek J, Haulon S, Zawadzki C, Jude B, Torpier G, Marx N, Staels B, Chinetti-Gbaguidi G. PPARgamma activation primes human monocytes into alternative M2 macrophages with anti-inflammatory properties. Cell Metab 2007;6:137–143
18. Sell H, Eckel J. Monocyte chemotactic protein-1 and its role in insulin resistance. Curr Opin Lipidol 2007;18:258–262
19. Gustafson B, Hammarstedt A, Andersson CX, Smith U. Inflamed adipose tissue: a culprit underlying the metabolic syndrome and atherosclerosis. Arterioscler ThrombVasc Biol 2007;27:2276–2283
20. Schadt EE, Lamb J, Yang X, Zhu J, Edwards S, Guhathakurta D, Sieberts SK, Monks S, Reitman M, Zhang C, Lum PY, Leonardson A, Thieringer R, Metzger JM, Yang L, Castle J, Zhu H, Kash SF, Drake TA, Sachs A, Lusis AJ. An integrative genomics approach to infer causal associations between gene expression and disease. Nat Genet 2005;37:710–717
21. Crass T, Raffetseder U, Martin U, Grove M, Klos A, Kohl J, Bautsch W. Expression cloning of the human C3a anaphylatoxin receptor (C3aR) from differentiated U-937 cells. Eur J Immunol 1996;26:1944–1950
22. Gasque P, Singhrao SK, Neal JW, Wang P, Sayah S, Fontaine M, Morgan BP. The receptor for complement anaphylatoxin C3a is expressed by myeloid cells and nonmyeloid cells in inflamed human central nervous system: analysis in multiple sclerosis and bacterial meningitis. J Immunol 1998;160:3543–3554
23. Martin U, Bock D, Arseniev L, Tornetta MA, Ames RS, Bautsch W, Kohl J, Ganser A, Klos A. The human C3a receptor is expressed on neutrophils and monocytes, but not on B or T lymphocytes. J Exp Med 1997;186:199–207
24. Zwirner J, Werfel T, Wilken HC, Theile E, Gotze O. Anaphylatoxin C3a but not C3a(desArg) is a chemotaxin for the mouse macrophage cell line J774. Eur J Immunol 1998;28:1570–1577
25. Takabayashi T, Shimizu S, Clark BD, Beinborn M, Burke JF, Gelfand JA. Interleukin-1 upregulates anaphylatoxin receptors on mononuclear cells. Surgery 2004;135:544–554
26. Oksjoki R, Laine P, Helske S, Vehmaan-Kreula P, Mayranpaa MI, Gasque P, Kovanen PT, Pentikainen MO. Receptors for the anaphylatoxins C3a and C5a are expressed in human atherosclerotic coronary plaques. Atherosclerosis 2007;195:90–99
27. Lattin J, Zidar DA, Schroder K, Kellie S, Hume DA, Sweet MJ. G-protein-coupled receptor expression, function, and signaling in macrophages. J Leuk Biol 2007;82:16–32
28. Lattin JE, Schroder K, Su AI, Walker JR, Zhang J, Wiltshire T, Saijo K, Glass CK, Hume DA, Kellie S, Sweet MJ. Expression analysis of G protein-coupled receptors in mouse macrophages. Immunome Res 2008;4:5
29. Yang Y, Lu HL, Zhang J, Yu HY, Wang HW, Zhang MX, Cianflone K. Relationships among acylation stimulating protein, adiponectin and complement C3 in lean vs obese type 2 diabetes. Int J Obes (Lond) 2006;30:439–446
30. Weyer C, Tataranni PA, Pratley RE. Insulin action and insulinemia are closely related to the fasting complement C3, but not acylation stimulating protein concentration. Diabetes Care 2000;23:779–785
31. Pomeroy C, Mitchell J, Eckert E, Raymond N, Crosby R, Dalmasso AP. Effect of body weight and caloric restriction on serum complement proteins, including Factor D/adipsin: studies in anorexia nervosa and obesity. Clin Exp Immunol 1997;108:507–515
32. Mantov S, Raev D. Additive effect of diabetes and systemic hypertension on the immune mechanisms of atherosclerosis. Int J Cardiol 1996;56:145–148
33. Figueredo A, Ibarra JL, Bagazgoitia J, Rodriguez A, Molino AM, Fernandez-Cruz A, Patino R. Plasma C3d levels and ischemic heart disease in type II diabetes. Diabetes Care 1993;16:445–449
34. Ylitalo K, Porkka KV, Meri S, Nuotio I, Suurinkeroinen L, Vakkilainen J, Pajukanta P, Viikari JS, Peltonen L, Ehnholm C, Taskinen MR. Serum complement and familial combined hyperlipidemia. Atherosclerosis 1997;129:271–277
35. Folch J, Lees M, Sloane Stanley GH. A simple method for the isolation and purification of total lipides from animal tissues. J Biol Chem 1957;226:497–509
36. Mantovani A, Sica A, Locati M. Macrophage polarization comes of age. Immunity 2005;23:344–346
37. Gordon S. Macrophage-restricted molecules: role in differentiation and activation. Immun Lett 1999;65:5–8
38. Tontonoz P, Spiegelman BM. Fat and beyond: the diverse biology of PPARgamma. Annu Rev Biochem 2008;77:289–312
39. Heilbronn LK, Campbell LV. Adipose tissue macrophages, low grade inflammation and insulin resistance in human obesity. Curr Pharm Design 2008;14:1225–1230
40. Patsouris D, Li PP, Thapar D, Chapman J, Olefsky JM, Neels JG. Ablation of CD11c-positive cells normalizes insulin sensitivity in obese insulin resistant animals. Cell Metab 2008;8:301–309
41. National Institutes of Health. Clinical trials on salsalate [article online], 2008. Available from http://clinicaltrials.gov/ct2/results?intr=%22Salsalate%22. Accessed 9 December 2008
42. Fleischman A, Shoelson SE, Bernier R, Goldfine AB. Salsalate improves glycemia and inflammatory parameters in obese young adults. Diabetes Care 2008;31:289–294
43. Goldfine A, Silver R, Shoelson S. Use of salsalate to target inflammation of insulin resistance and type 2 diabetes. Clin Translat Sci 2008;1:36–43
44. MacLaren R, Cui W, Cianflone K. Adipokines and the immune system: an adipocentric view. Adv Exp Med Biol 2008;632:1–21
45. Murray I, Sniderman AD, Cianflone K. Mice lacking acylation stimulating protein (ASP) have delayed postprandial triglyceride clearance. J Lipid Res 1999;40:1671–1676
46. Murray I, Sniderman AD, Havel PJ, Cianflone K. Acylation stimulating protein (ASP) deficiency alters postprandial and adipose tissue metabolism in male mice. J Biol Chem 1999;274:36219–36225
47. Xia Z, Sniderman AD, Cianflone K. Acylation-stimulating protein (ASP) deficiency induces obesity resistance and increased energy expenditure in ob/ob mice. J Biol Chem 2002;277:45874–45879